HgCdTe Focal Plane Arrays for Dual-Color Mid- and Long-Wavelength Infrared Detection

E.P.G. SMITH,[1,4] L.T. PHAM,[1] G.M. VENZOR,[1] E.M. NORTON,[1] M.D. NEWTON,[1] P.M. GOETZ,[1] V.K. RANDALL,[1] A.M. GALLAGHER,[1] G.K. PIERCE,[1] E.A. PATTEN,[1] R.A. COUSSA,[1] K. KOSAI, W.A. RADFORD,[1] L.M. GIEGERICH,[1] J.M. EDWARDS,[1] S.M. JOHNSON,[1] S.T. BAUR,[1] J.A. ROTH,[2] B. NOSHO,[2] T.J. DE LYON,[2] J.E. JENSEN,[2] and R.E. LONGSHORE[3]

1.—Raytheon Vision Systems, Goleta, CA 93117. 2.—HRL Laboratories, LLC, Malibu, CA 90265. 3.—Raytheon Missile Systems, Tucson, AZ 85706. 4.—E-mail: edward_p_smith@raytheon.com

Raytheon Vision Systems (RVS, Goleta, CA) in collaboration with HRL Laboratories (Malibu, CA) is contributing to the maturation and manufacturing readiness of third-generation, dual-color, HgCdTe infrared staring focal plane arrays (FPAs). This paper will highlight data from the routine growth and fabrication of 256 × 256 30-μm unit-cell staring FPAs that provide dual-color detection in the mid-wavelength infrared (MWIR) and long wavelength infrared (LWIR) spectral regions. The FPAs configured for MWIR/MWIR, MWIR/LWIR, and LWIR/LWIR detection are used for target identification, signature recognition, and clutter rejection in a wide variety of space and ground-based applications. Optimized triple-layer heterojunction (TLHJ) device designs and molecular beam epitaxy (MBE) growth using in-situ controls has contributed to individual bands in all dual-color FPA configurations exhibiting high operability (>99%) and both performance and FPA functionality comparable to state-of-the-art, single-color technology. The measured spectral cross talk from out-of-band radiation for either band is also typically less than 10%. An FPA architecture based on a single-mesa, single-indium bump, and sequential-mode operation leverages current single-color processes in production while also providing compatibility with existing second-generation technologies.

Key words: Dual-color, focal plane array (FPA), mid-wavelength infrared (MWIR), long-wavelength infrared (LWIR), molecular beam epitaxy (MBE)

INTRODUCTION

Mercury cadmium telluride (HgCdTe) is the highest performing and most versatile material available for infrared focal plane array (FPA) fabrication.[1–3] The fundamental HgCdTe material properties that are advantageous for infrared detection include high quantum efficiency, small effective mass, large electron-to-hole mobility ratio, and long minority-carrier lifetime.[1] The material's adjustable (direct interband transition) energy gap with sensitivity spanning from the short wavelength infrared (SWIR) to very long wavelength infrared (VLWIR) bands of the infrared spectrum (1–20 μm) also enable a tremendous number of applications to be realized using advanced material growth methods and different detector designs. Current second-generation HgCdTe FPA technology, two-dimensional detector arrays sensitive to one spectral region of the infrared spectrum mated to a readout integrated circuit (ROIC), is being readily produced with increasing array sizes and cutoff wavelengths extending further into the VLWIR range.[2] Following a decade of development, third-generation multispectral or dual-color FPAs are now approaching manufacturing readiness. These FPAs address increasing demand to expand the capabilities of existing single-color systems as well as the development of new and more sophisticated infrared systems.[4]

(Received October 2, 2003; accepted December 1, 2003)

Integrated dual-color infrared detection, where each pixel of a single FPA can detect two distinct spectral bands, has the potential to translate in to system weight, cost, and performance advantages.[3] Multispectral systems using single-color FPAs often support a wide range of auxiliary equipment to focus images on to more than one FPA that respond to different infrared wavelengths. This equipment may include beam splitters, lenses, prisms, and bandpass filters. The availability of spectral information from a second spectral band enables discrimination of absolute temperature and unique signatures of objects in a scene.[4] When coupled with advanced signal-processing algorithms, dual-color infrared detection provides improved sensitivity compared to that of single-color devices in addition to the fact that it is possible for multispectral system requirements to be consolidated in to fewer FPAs or even a single FPA. Multispectral infrared detection can be employed in space and ground-based imaging for the military and civilian communities, where civilian applications may include earth and planetary remote sensing and astronomy.[5]

Raytheon Vision Systems (RVS) in collaboration with HRL Laboratories currently performs low-rate production of 256 × 256 30-μm unit-cell staring HgCdTe FPAs configured for dual-color imaging in the mid-wavelength infrared (MWIR) and long wavelength infrared (LWIR) spectral regions. The production capability at RVS encompasses detector design and material growth, wafer processing, FPA hybridization to ROICs, testing, and packaging. A feature of the dual-color FPAs being produced at RVS is that they can be seamlessly inserted into existing single-color dewars and systems with only minor modifications to FPA control and signal-processing electronics. This paper presents an overview of the capability at RVS to meet manufacturing and development requirements for third-generation, dual-color detectors and a discussion related to detector architecture and operation, material growth, FPA fabrication, and detector and FPA performance.

DETECTOR ARCHITECTURE AND OPERATION

The approach undertaken by RVS for a monolithic, dual-color detector FPA is an n-p^+-n HgCdTe triple-layer heterojunction (TLHJ), back-to-back p^+-n photodiode structure grown by molecular beam epitaxy (MBE) on a (211)-oriented cadmium zinc telluride (CdZnTe) substrate. In this design, the longer wavelength detector is inverted into an n-p^+ device that is grown on top of the shorter wavelength detector where the p^+ layer of both detectors is merged to form the n-p^+-n structure. The entire structure can be grown in a single growth run, and the n-type absorber layers can span any of the HgCdTe compositions that allow detection in the SWIR to VLWIR infrared spectral regions. Operated with backside illumination, the first n-type layer absorbs the shorter wavelength (Band 1) radiation, which is sensed by the bottom photodiode. Longer wavelength (Band 2) radiation passes through the bottom n-type absorber and middle p^+ layer and is detected by the top photodiode.

The RVS architecture for small pixel 30-μm unit-cell FPAs leaves the p^+ layer floating, and the polarity of the voltage bias at the single pixel contact selects the spectral sensitivity by reverse-biasing the p-n junction of interest. Illustrated in Fig. 1 is a scanning electron micrograph image and cross-section schematic of a 30-μm unit-cell, single-mesa, single-contact TLHJ dual-color detector, in addition to the typical current-voltage (I-V) characteristic for this detector design. A positive (negative) operating bias voltage at the pixel contact with respect to the FPA common-ground contact provides reverse bias to the Band 2 (Band 1) p-n junction while forward biasing the Band 1 (Band 2) p-n junction for detection of longer (shorter) wavelength radiation.

The single-mesa, single-contact dual-color architecture used by RVS provides perfect pixel registration and close to 100% optical fill factor for each detection band while also contributing to a combination of performance, manufacturing, and technology development advantages. The single contact re-

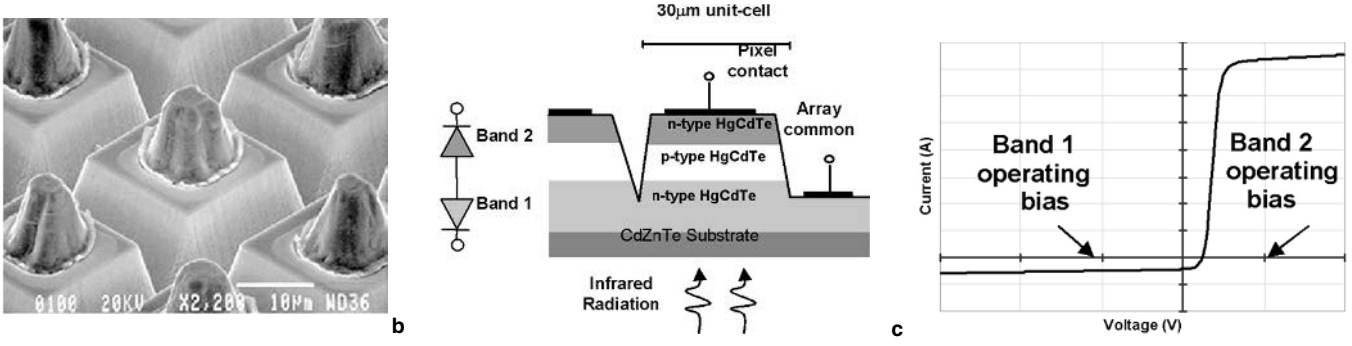

a b c

Fig. 1. (a) A SEM image, (b) cross-section schematic, and (c) typical I-V characteristic for a single-mesa, single-indium bump, dual-color HgCdTe, TLHJ 30-μm unit-cell detector design. With the appropriate polarity and voltage bias at the pixel contact, the Band 1 and Band 2 p-n junctions respond to shorter and longer wavelength infrared radiation, respectively. Deep anisotropic mesa etching is required to ensure that both the Band 1 and Band 2 p-n junctions are isolated between adjacent pixels.

quires only one indium bump per unit cell to be used in hybridizing the FPA to it ROIC. This approach capitalizes on the mature second-generation, p^+-on-n double-layer heterojunction (DLHJ) technology developed at RVS using liquid-phase epitaxy (LPE) grown HgCdTe on CdZnTe and the emerging DLHJ MBE-on-Si technology, which are both based on a similar single-mesa, single-indium bump architecture.[6,7] Minimizing indium bump density is a practical approach for building on process commonalities with second-generation technologies as well as facilitating the future development of larger format dual-color arrays with reduced unit-cell size. In addition, depending on application and performance specifications, "frame-sequential" dual-color detection can be performed using second-generation single-color ROICs. In frame-sequential operation, the integrating detection band is determined by the polarity of the detector bias, which is inverted in alternating frames to produce a dual-color image with a frame-time interlace period. Raytheon Vision Systems has also developed time-division multiplexing ROIC technology to provide "frame-simultaneous" or pseudo-simultaneous detection by rapidly switching the voltage bias at the pixel contact to allow near simultaneous integration of Band 1 and Band 2 signals.

MATERIAL GROWTH

The MBE technology at HRL Laboratories has evolved in to a mature state that routinely produces n-p^+-n HgCdTe TLHJ dual-color device structures that meet a wide variety of material design specifications. The MBE systems equipped with Hg, Te, and CdTe sources are used for HgCdTe TLHJ growth, and system details and growth conditions pertinent to TLHJ growth has been reported in previous publications.[8–10] Continuous improvements in MBE growth of TLHJ layers has resulted in increasing wafer sizes with better cutoff uniformity and lower numbers of defects. These are all key factors that contribute to improvements in wafer and FPA yield that enable demand for higher performance and reduced product costs to be met. Substrate sizes have increased from 3 cm × 3 cm to 4 cm × 4 cm with average macrodefect (void and micro-void) density and cutoff uniformity reduced to less than 1,000 per cm^2 and $\Delta\lambda_c = 0.5$ μm, respectively, for 4 cm × 4 cm wafers. Illustrated in Fig. 2 are statistics and numbers of deliverable MBE-grown HgCdTe TLHJ wafers for FPA fabrication in recent years.

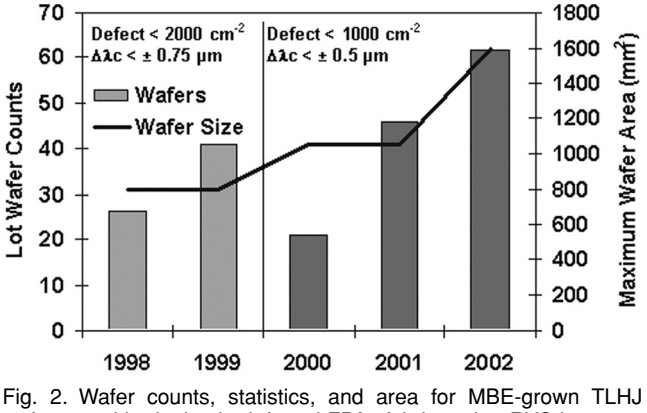

Fig. 2. Wafer counts, statistics, and area for MBE-grown TLHJ wafers used in dual-color infrared FPAs fabricated at RVS in recent years.

Optimized, MBE-grown HgCdTe, TLHJ device architectures may contain up to five or more layers where the composition and doping of each layer is different from the preceding layer. Doping of both n- and p-type layers is performed in situ during growth using In and As dopants, respectively. This approach ensures that the entire structure, incorporating the junction and absorber layers, is grown in a single growth run, which alleviates the need for additional junction-formation techniques following growth and during wafer processing.

The CdTe/HgTe alloy composition or x value of the n-type absorber layers determines the spectral cutoff characteristics of the detector in both detection bands. It is necessary to have precise control of this growth variable to guarantee that individual growth runs meet desired cutoff targets as well as ensuring run-to-run growth uniformity. In-situ spectral ellipsometry (SE) is a technique that has proven valuable in the development of deposition processes for HgCdTe layers and provides the ability to monitor and accurately control the composition of a growing layer in real time.[11] As illustrated in Fig. 3, the inclusion of SE with feedback control systems to adjust growth parameters has allowed an average standard deviation of 0.14 from target cutoff wavelengths in 10.5-μm absorber layers to be achieved.

The density of void and micro-void macro defects and threading dislocations are two material properties that can influence dark current performance and, therefore, operability of epitaxially grown heterojunction detectors.[12] Threading dislocations are typically

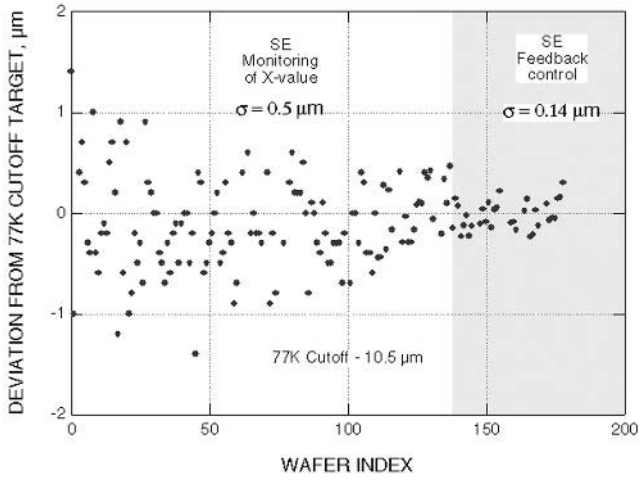

Fig. 3. The standard deviation of target cutoff wavelengths as a function of HgCdTe wafer index before and after the inclusion of SE with feedback control systems to adjust growth parameters in 10.5-μm (77K cutoff wavelength) absorber layers.

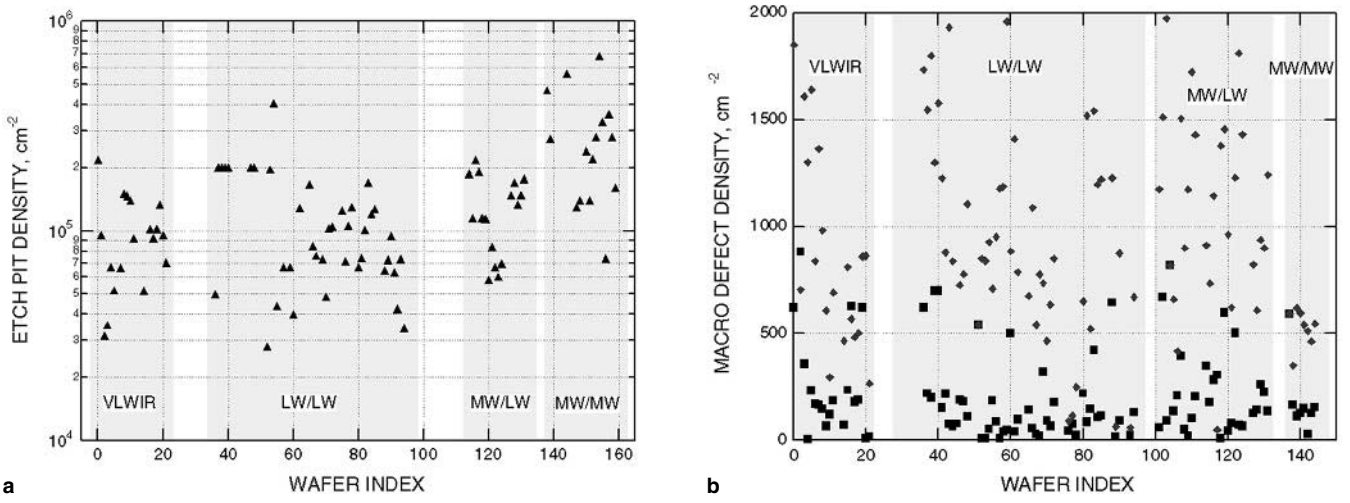

Fig. 4. Measured (a) EPD and (b) macro defect density as a function of wafer index for various HgCdTe detector configurations with different device designs and cutoff wavelengths.

observed in HgCdTe layers by the application of a decorative defect etch to reveal an etch pit density (EPD).[8,12] As shown in Fig. 4, macrodefect and EPD levels can vary depending on the composition and type of device structure grown.

FPA FABRICATION

The fabrication of small pixel dual-color HgCdTe FPAs based on an MBE-grown TLHJ architecture incorporates mesa delineation of each pixel, deposition of passivation and contact-metal layers, and indium-bump processing for hybridization of the FPA to a ROIC. In dual-color HgCdTe TLHJ FPA fabrication it is necessary to isolate the p-n junction of both wavelength detection bands in each pixel, which can require mesa etch depths up to 15 μm. Dry plasma etching is one of the most demanding areas of HgCdTe device fabrication, but it can provide significant benefits for mesa delineation, such as anisotropic profiles, greater uniformity, and improved dimensional control when compared with traditional wet-chemical etching.[13,14] The HgCdTe dry plasma etching procedures have been successfully developed by RVS to achieve deep high-aspect-ratio mesa profiles that are compatible with subsequent process steps in a FPA fabrication sequence without compromising fill factors in TLHJ detector designs.

Raytheon Vision Systems is actively developing advanced HgCdTe dry-etching processes based on high-density plasma (HDP) etching techniques that include electron cyclotron resonance (ECR) and inductively coupled plasma (ICP). The HDP techniques aim to decouple plasma generation and ion energy by using an additional source remote from the radio-frequency powered wafer electrode to generate a plasma. Independent control of the plasma and bombardment energy allows for the generation of HDP while limiting the energy of ions impinging on the wafer surface.[15] The ICP technique has been identified in the semiconductor industry as a more attractive choice for manufacturing applications because of easier scale up to larger wafer sizes and greater automation capability than ECR.[16,17] Consequently, ICP tools that deliver high plasma uniformity over large wafer sizes are seeing widespread application in silicon and III-V semiconductor technology.[15]

Work performed at RVS on HgCdTe HDP mesa etching with ECR and ICP techniques has identified ICP etching capable of producing up to a factor of 5 reduction in lateral mask erosion during etching, improved etch-depth uniformity, and less significant etch-lag effects.[15,18] These benefits provide improved process capability to delineate high-aspect-ratio mesa geometries to achieve high fill-factor FPAs while minimizing exposure of HgCdTe material to ion bombardment from prolonged dry-etching procedures that may adversely affect detector performance. Illustrated in Fig. 5 is a scanning electron microscopy (SEM) image of deep, mesa trench profiles defined in HgCdTe using ICP etching and a graph describing etch depth for different trench widths as a function of process time. The graph illustrates that the onset of etch lag, where the etch depth or etch rate for smaller trench dimensions deviates from larger trench dimensions, is not prominent for deep, mesa trench profiles up to 14 μm in etch depth.

DETECTOR AND FPA PERFORMANCE

The RVS HgCdTe dual-color detector technology has the capability to provide combinations of any two nonoverlapping spectral bands in the SWIR to VLWIR spectral regions. Filters can be used to further define the spectral window of interest and eliminate undesired spectral regions, such as atmospheric absorption bands. Figure 6 provides examples of spectral response for MWIR and LWIR HgCdTe, dual-color detector configurations. All wavelength configurations in Fig. 8 exhibit sharp spectral characteristics, and the measured response from out-of-band radiation, commonly referred to as

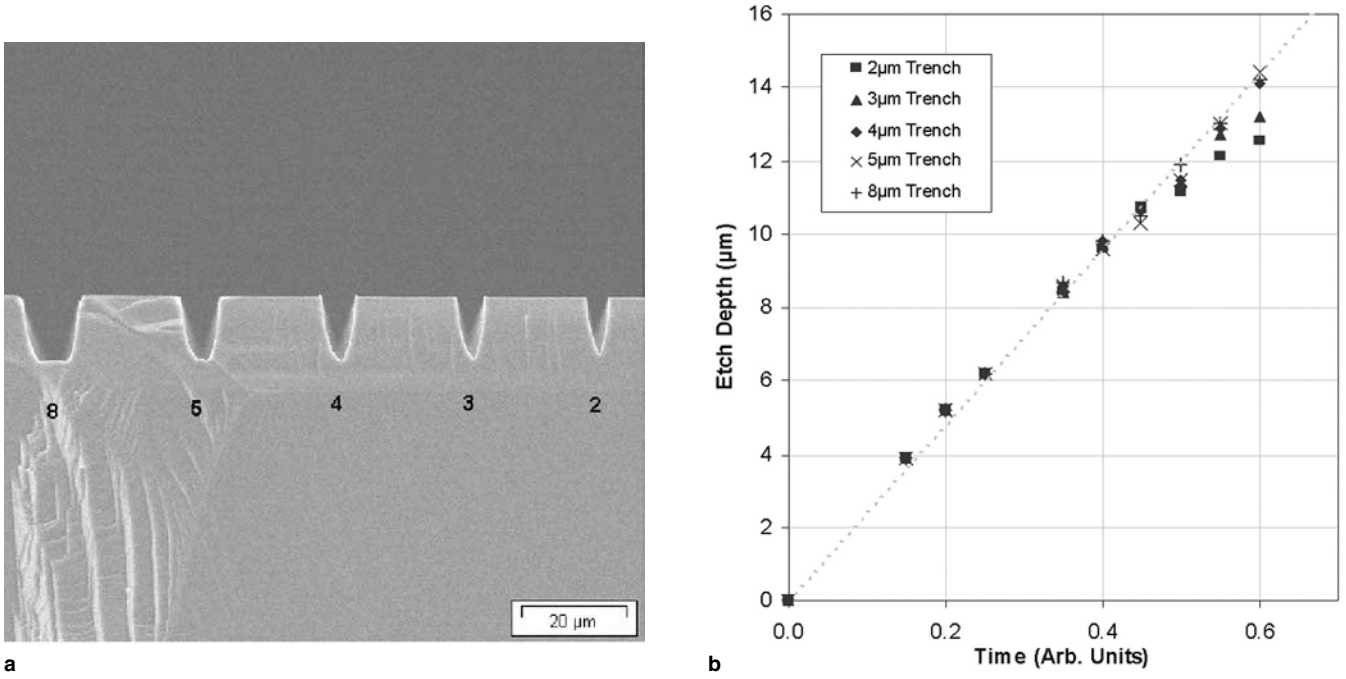

Fig. 5. A SEM image of deep, mesa trench profiles defined in HgCdTe using ICP etching and a graph describing etch depth for different trench widths as a function of process time. Each trench profile in the SEM image is annotated with the photomask dimension used to define the trench opening in the mask layer prior to etching and corresponds to the trench dimension described in the graph. The dotted line in the graph is a linear fit to the etch depth measured for the 8-µm trench and represents the absence of etch lag. This highlights the fact that etch lag is not a feature prominently observed over a wide range of trench dimensions up to an etch depth of approximately 14 µm.

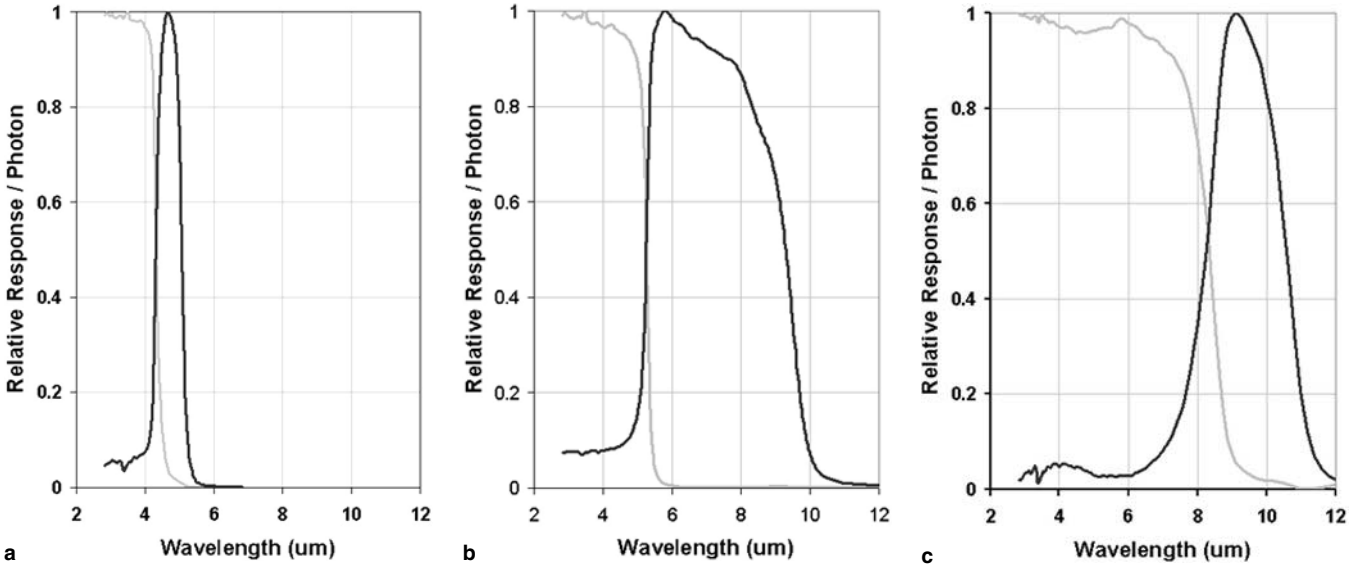

Fig. 6. Spectral response in units of relative response per photon as a function of wavelength for (a) MWIR/MWIR, (b) MWIR/LWIR, and (c) LWIR/LWIR detector configurations for dual-color HgCdTe 256 × 256 30-µm unit-cell FPAs.

"cross talk," for either band is less than 10%. Optimization of cross talk in TLHJ structures is largely dependent on detector design and precise material growth to ensure that the n-type absorber and p-type cap layers are of the appropriate thickness, composition, and doping. The Band 1 absorber layer tends to absorb nearly 100% of the shorter wavelengths and, coupled with the wider bandgap and highly doped p-type layer, ensures that the measured response from out-of-band radiation in Band 2 is typically less than that measured for out-of-band radiation in Band 1.

The performance and operability of the dual-color HgCdTe TLHJ detectors and FPAs fabricated at RVS consistently exhibit high performance for all MWIR and LWIR configurations. The operating temperature, quantum efficiency, leakage current, and pixel operability of the best performing dual-color FPAs is comparable to state-of-the-art, single-color detectors currently in fabrication. A summary of

Table I. Typical Measured Performance Parameters for Single- and Dual-Color HgCdTe MWIR and LWIR Detector Configurations for 256 × 256 30-μm Unit-Cell FPAs

256 × 256 30-μm Unit-Cell Performance Parameters	DLHJ Single Color		TLHJ Sequential Dual Color					
	MWIR	LWIR	MWIR/MWIR		MWIR/LWIR		LWIR/LWIR	
Spectral band	MWIR	LWIR	Band 1	Band 2	Band 1	Band 2	Band 1	Band 2
78-K cutoff (μm)	5	10	4	5	5	10	8	10
Operating temperature (K)	78	78	120	120	70	70	70	70
Cross talk (%)	NA	NA	<5	<10	<5	<10	<5	<10
Quantum efficiency (%)	>70	>70	>70	>65	>70	>50	>70	>50
R_0A 0 Field of view (Ωcm^2)	$>1 \times 10^7$	>500	NA	NA	NA	NA	NA	NA
R_rA 0 Field of view (Ωcm^2)	NA	NA	6×10^5	2×10^5	1×10^6	2×10^2	5×10^4	5×10^2
Interconnect operability (%)	>99.9	>99.9	>99.9	>99.9	>99.9	>99.9	>99.9	>99.9
Response operability (%)	>99	>98	>99	>97	>99	>97	>98	>95

typical performance in various single- and dual-color MWIR and LWIR detector configurations for 30-μm unit-cell 256 × 256 FPAs is presented in Table I. The performance parameters include cutoff wavelength, operating temperature, cross talk, quantum efficiency, R_0A and R_rA, interconnect, and pixel operability. The R_rA (resistance-area product at nonzero bias) is a commonly used figure of merit for sequential, dual-color TLHJ detector structures that exhibit back-to-back diode I-V characteristics, as opposed to R_0A (resistance-area product measured at zero bias) for single-color detectors. These differences make comparisons between sequential dual-color detector performance and trend-line, single-color detector performance, such as R_0A product variation with wavelength at a given temperature, difficult to achieve in practice. Simultaneous dual-color detector performance, where an additional contact is made to the p-type layer to independently bias the Band 1 and Band 2 p-n junctions using TLHJ structures grown by LPE, has previously been shown to be comparable to single-color trend-line data.[19]

The quantum efficiency values, presented in Table I, are typical for individual detectors or FPAs evaluated with antireflection coatings. The application of antireflection coatings can contribute to greater than 15% improvement in quantum efficiency performance. Illustrated in Fig. 7 are typical histogram plots of effective quantum efficiency extracted from measured responsivity for TLHJ HgCdTe 256 × 256 30-μm unit-cell sequential dual-color FPAs in two different MWIR and LWIR configurations. It can be seen from this figure that the dual-color histogram plots show comparable quantum efficiency and distribution to the histogram plot of effective quantum efficiency for a typical LPE-grown LWIR DLHJ 256 × 256 30-μm unit-cell single-color FPA.

The interconnect operability between corresponding FPA and ROIC pixels following hybridization in 30-μm unit-cell 256 × 256 single- and dual-color FPA formats typically exceeds 99.9% (fewer than 66 inoperable pixels) and is not a factor that significantly influences FPA pixel operability. In Table I, FPA operability is defined for pixels with a responsivity value

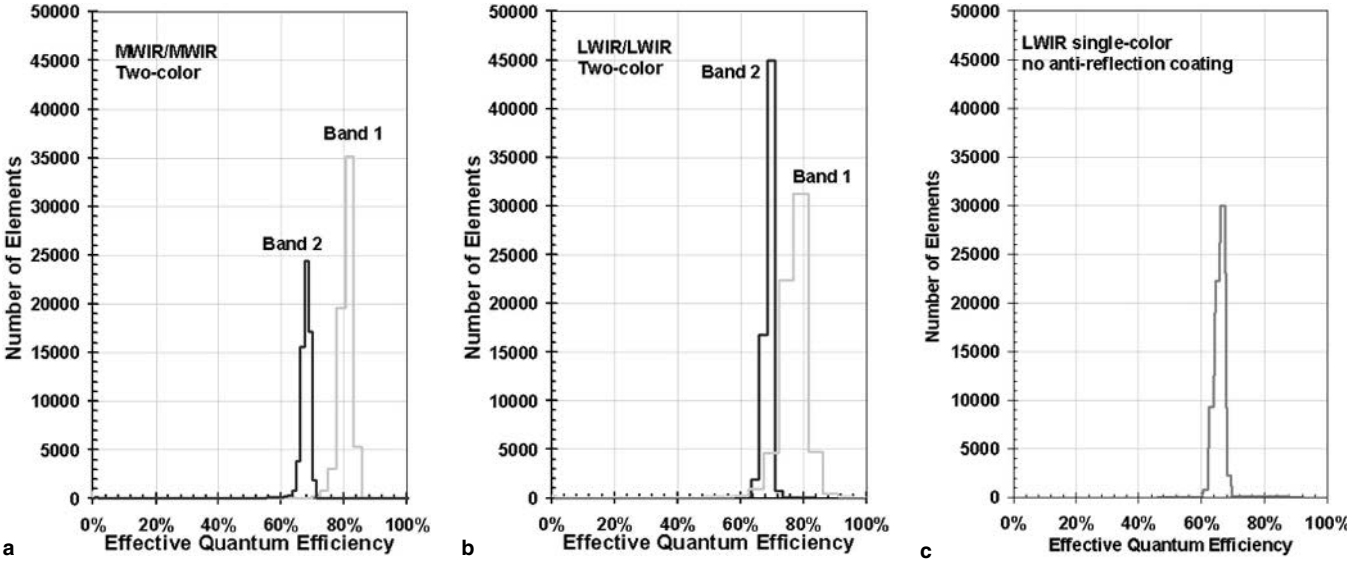

Fig. 7. Histogram plots of effective quantum efficiency for dual-color HgCdTe TLHJ 256 × 256 30-μm unit-cell FPAs MWIR/MWIR and LWIR/LWIR configurations and a single-color HgCdTe DLHJ 256 × 256 30-μm unit-cell LWIR FPA.

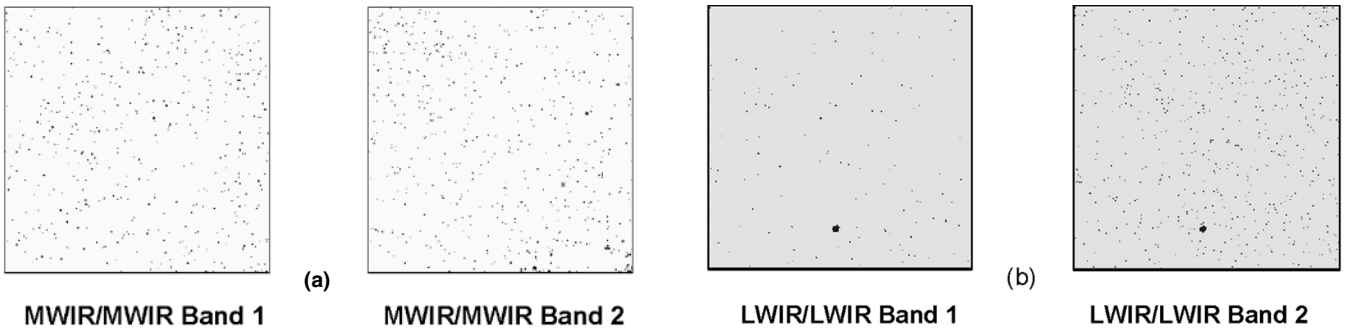

Fig. 8. Spatial pixel operability maps for dual-color HgCdTe TLHJ 256 × 256 30-μm unit-cell FPAs in (a) a MWIR/MWIR configuration with greater than 99% response operability in both wavelength bands at an operating temperature of 115 K and (b) a LWIR/LWIR configuration also with greater than 99% response operability in both wavelength bands at an operating temperature of 70 K. It should be noted that the inoperable pixels (in black) account for only a few percent of the total FPA pixel count, and it is significant that the inoperable pixels are randomly distributed with no large cluster defect regions.

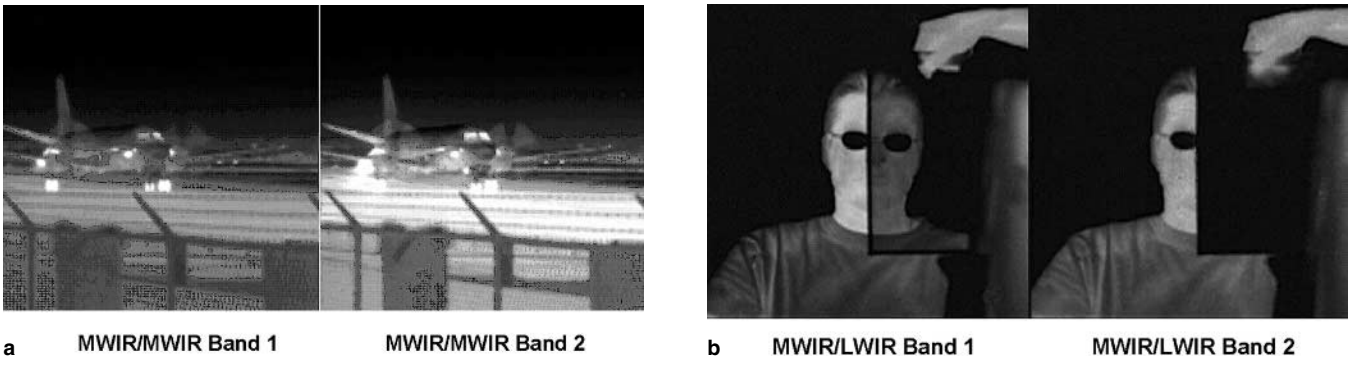

Fig. 9. Infrared images taken using dual-color HgCdTe TLHJ 256 × 256 30-μm unit-cell FPAs for (a) MWIR/MWIR and (b) MWIR/LWIR detector configurations.

greater than half or less than twice the average array responsivity. Operability and response uniformity (standard deviation of array responsivity divided by average array responsivity) in manufactured FPAs across all MWIR and LWIR bands is consistently observed to be greater than 95% and less than 0.15, respectively. In best performing FPAs, operability greater than 99% and response uniformity less than 0.06 has been recorded for MWIR and LWIR bands. Examples of spatial pixel operability maps for two 256 × 256 30-μm unit-cell FPAs in MWIR/MWIR and LWIR/LWIR configurations are shown in Fig. 8. The operability of the dual-color detector configurations demonstrates a wide performance margin against operating temperature. Minimal change in Band 1 and Band 2 pixel operability is observed for 70–120 K operating temperatures in MWIR/MWIR configurations and for 70–90 K operating temperatures in MWIR/LWIR and LWIR/LWIR configurations.

High-quality imaging with both frame-sequential and frame-simultaneous ROIC designs has been achieved using various dual-color detector architectures. Camera images for MWIR/MWIR and MWIR/LWIR detector configurations using frame-simultaneous techniques are illustrated in Fig. 9.

SUMMARY AND CONCLUSIONS

This paper has presented an overview of the capabilities at RVS and HRL Laboratories for the design, modeling, growth, and fabrication of third-generation dual-color HgCdTe infrared staring FPAs. The single-mesa, single-indium bump detector architecture developed at RVS based on a MBE-grown HgCdTe TLHJ device design coupled with advanced fabrication techniques has numerous advantages for manufacturing and development of multispectral infrared FPAs. The routine growth and fabrication of 256 × 256 30-μm unit-cell infrared staring FPAs that provide dual-color detection in the MWIR and LWIR spectral regions is an indication that third-generation dual-color detectors are approaching higher rate production and manufacturing readiness. The best performing dual-color FPAs being produced at RVS exhibit out-of-band spectral cross talk below 10%, 99.9% interconnect operability, and 99% response operability that is comparable to state-of-the-art, single-color technology. Ongoing development of material growth and fabrication processes will translate to further improvements in dual-color FPA performance. It will also facilitate the development of larger dual-color FPA sizes with reduced unit-cell dimensions that incorporate device designs and configurations to accommodate a wide range of SWIR to VLWIR spectral bands for a variety of applications.

ACKNOWLEDGEMENTS

The authors acknowledge a productive customer and collaborative relationship with Jim Waterman,

Naval Research Laboratory, as well as the Night Vision Electronic Sensors Directorate, Penn State ARL Electro-Optics Center, and Raytheon Missile Systems. We gratefully acknowledge Frank Aguilar, Douglas Bentley, Aimee Buell, Jana Choquette-Ortega, John Deloo, Roger Graham, Virginia Harper, Malcolm Kamdar, Valerie Lee, Octavio Lira, Salvador Ortega, and Dean Weideman whose sustained work efforts make this technology development successful. This work was supported by Raytheon IR&D.

REFERENCES

1. S.C. Shen, *Microelectron. J.* 25, 713 (1994).
2. A. Rogalski, *Infrared Phys. Technol.* 41, 213 (2000).
3. A. Rogalski, *Appl. Phys. Lett.* 93, 4355 (2003).
4. W. Cabanski, R. Brieter, R. Koch, K.-H. Mauk, W. Rode, J. Ziegler, H. Schneider, M. Walther, and R. Oelmaier, *Proc. SPIE* 4369, 547 (2001).
5. P. Ferret, J.P. Zanatta, R. Hamelin, S. Cremer, A. Million, M. Wolny, and G. Destefanis, *J. Electron. Mater.* 29, 641 (2000).
6. T. Tung, L.V. DeArmond, R.F. Herald, P.E. Herning, M.H. Kalisher, D.A. Olson, R.F. Risser, A.P. Stevens, and S.J. Tighe, *Proc. SPIE* 1735, 109 (1992).
7. J.B. Varesi, R.E. Bornfreund, A.C. Childs, W.A. Radford, K.D. Maranowski, J.M. Peterson, S.M. Johnson, L.M. Giegerich, T.J. de Lyon, and J.E. Jensen, *J. Electron. Mater.* 30, 566 (2001).
8. R.D. Rajavel, D.M. Jamba, O.K. Wu, J.E. Jensen, J.A. Wilson, E.A. Patten, K. Kosai, P. Goetz, G.R. Chapman, and W.A. Radford, *J. Cryst. Growth* 157/176, 653 (1997).
9. R.D. Rajavel, O.K. Wu, J.E. Jensen, C.A. Cockrum, G.M. Venzor, E.A. Patten, P.M. Goetz, D. Leonard, and S.M. Johnson, *Mater. Res. Soc. Symp. Proc.* 421, 335 (1996).
10. S.M. Johnson et al., *J. Electron. Mater.* 29, 680 (2000).
11. L.A. Almeida, M. Thomas, W. Larsen, K. Spariosu, D.D. Edwall, J.D. Benson, W. Mason, A.J. Stoltz, and J.H. Dinan, *J. Electron. Mater.* 31, 669 (2002).
12. S.M. Johnson, D.R. Rhiger, J.P. Rosbeck, J.M. Peterson, S.M. Taylor, and M.E. Boyd, *J. Vac. Sci. Technol. B* 10, 1499 (1992).
13. R.C. Keller, M. Seelmann-Eggebert, and H.J. Richter, *J. Electron. Mater.* 25, 1270 (1996).
14. R.C. Keller, M. Seelmann-Eggebert, and H.J. Richter, *J. Electron. Mater.* 24, 1155 (1995).
15. E.P.G. Smith, J.K. Gleason, L.T. Pham, E.A. Patten, and M.S. Welkowsky, *J. Electron. Mater.* 32, 816 (2003).
16. R.J. Shul, G.B. McClellan, R.D. Briggs, D.J. Rieger, S.J. Pearton, C.R. Abernathy, J.W. Lee, C. Constantine, and C. Barratt, *J. Vac. Sci. Technol. A* 15, 633 (1997).
17. L. Zhang, L.F. Lester, R.J. Shul, C.G. Willison, and R.P. Leavitt, *J. Vac. Sci. Technol. B* 17, 965 (1999).
18. E.P.G. Smith et al., *J. Electron. Mater.* 32, 821 (2003).
19. J.A. Wilson et al., *Proc. SPIE* 2274, 117 (1994).